

Gigantic diphoton rate of heavy Higgs bosons in the aligned two Higgs doublet models with small $\tan\beta$

Jeonghyeon Song^{*} and Yeo Woong Yoon[†]*School of Physics, KonKuk University, Seoul 143-701, Korea*

(Received 1 January 2015; published 22 June 2015)

We study the implications of the LHC heavy neutral Higgs boson search data on the aligned two Higgs doublet model with a softly broken Z_2 symmetry. When $\tan\beta$ is small, the gluon fusion production of the heavy CP -even scalar H^0 or the CP -odd scalar A^0 becomes large enough to constrain the model by the current $\gamma\gamma$, $\tau^+\tau^-$, and $t\bar{t}$ data. By reinvestigating the indirect constraints from $\Delta\rho$, $b \rightarrow s\gamma$, ΔM_{B_d} , R_b , ϵ_K , and the perturbativity of the running top quark Yukawa coupling, we find that the small $\tan\beta$ region is still allowed: for instance, $\tan\beta \gtrsim 0.6(0.5)$ for Type I and X (II and Y) for $m_{H^\pm} = 800$ GeV. We find that the current LHC results of the heavy Higgs searches at $\sqrt{s} = 8$ TeV are shown to put on more significant bounds. If $m_H \approx m_A$, the $t\bar{t}$ mode excludes $\tan\beta \lesssim 1.5$ for $m_{H,A} = 500$ –600 GeV in all four types, and the $\gamma\gamma$ and $\tau^+\tau^-$ modes exclude $\tan\beta \lesssim 1$ –3 ($\tan\beta \lesssim 3$ –10) for $m_{H,A} = 150$ –340 GeV in Types I, II, and Y (Type X).

DOI: [10.1103/PhysRevD.91.113012](https://doi.org/10.1103/PhysRevD.91.113012)

PACS numbers: 14.80.Bn, 14.80.Ec, 12.60.Fr

I. INTRODUCTION

The discovery of a scalar boson with mass around 125 GeV at the LHC completes the standard model (SM) of particle physics as explaining the electroweak symmetry breaking by the Higgs mechanism, the last missing piece of the puzzle [1]. This newly discovered scalar boson is very likely the SM Higgs boson. The diphoton rate, which showed some deviation from the SM prediction in 2013 analysis [2,3], approaches the SM value in 2014 analysis [4,5] by virtue of enormous experimental efforts to improve the diphoton mass resolution as well as the photon energy resolution.

The observation of the 125 GeV state through various decay channels clears up many ambiguities about the Higgs boson such as its mass, spin, and coupling strengths with the SM particles, giving us a direction of a way forward. With the observed mass of the SM-like Higgs boson, the electroweak precision data are now overconstrained. We have a large improvement in precision for the indirect measurement of the W boson mass and the electroweak mixing angle $\sin\theta_W$ [6,7]. Another direction is into the high energy front, where physics beyond the SM is believed to exist because of various problems of the SM such as the gauge hierarchy problem and the dark matter problem. Many new physics models have the extended Higgs sector and thus heavy Higgs bosons. The requirement to accommodate a SM-like Higgs boson constrains new physics models considerably [8–11]. For example, the observed Higgs boson mass around 125 GeV prefers the additional Higgs bosons within the reach of the LHC in order to avoid another fine-tuning problem.

ATLAS and CMS have searched the heavy Higgs-like states through various channels. The most stringent bounds are from its decay into ZZ [12,13]: if the heavy state is a SM-like Higgs boson, the $H \rightarrow ZZ \rightarrow 2\ell 2\nu$ mode excludes its mass below ~ 580 GeV [13]. Other channels such as $H \rightarrow WW \rightarrow \ell\nu\ell\nu$ [14], the dijet mode [15], the $\tau^+\tau^-$ mode [16], and the $t\bar{t}$ mode [17] have been also searched. Another efficient mode is into the diphoton, which played a central role in identifying the SM-like Higgs boson. Recently the ATLAS collaboration reported the search for the diphoton resonances in the mass range of 65–600 GeV at $\sqrt{s} = 8$ TeV [18], and the CMS reported the search in the 150–850 GeV range [19]. No additional resonance with significant evidence is observed. However, there are a few excesses with a 2σ local significance at $m_{\gamma\gamma} \approx 200$ GeV and $m_{\gamma\gamma} \approx 530$ GeV in the ATLAS result [18], and $m_{\gamma\gamma} \approx 570$ GeV in the CMS result [19].

A new physics model with extended Higgs sector gets influence by all of the heavy Higgs search in the ZZ , WW , $t\bar{t}$, $\tau^+\tau^-$, and $\gamma\gamma$ modes, as well as the observed SM-like Higgs boson data. A comprehensive study is required. The diphoton channel is expected to play a crucial role because of its high sensitivity over a wide mass range. Within a given new physics model, finding the parameter space sensitive to the diphoton rate and examining its compatibility with other heavy Higgs search limits are worthwhile. More radically, we may ask the question whether a new physics model can accommodate a *gigantic* diphoton rate since any of the diphoton resonances at 2σ level requires a huge rate compared with the SM Higgs boson at that mass. A rough estimate yields the signal strength to be of the order of 10 for $m_{\gamma\gamma} \approx 200$ GeV and of the order of 10^4 for $m_{\gamma\gamma} \approx 530$ GeV resonance.

^{*}jeonghyeon.song@gmail.com
[†]ywoon@kias.re.kr

Focused on two Higgs doublet model (2HDM) [20], we study the implication of the heavy Higgs searches at the LHC. As one of the simplest extensions of the SM, 2HDM has two complex Higgs doublets. There are five physical Higgs boson degrees of freedom: the light CP -even scalar h^0 , the heavy CP -even scalar H^0 , the CP -odd pseudoscalar A^0 , and two charged Higgs bosons H^\pm . The model has drawn a lot of interest recently. In the literature, there are various studies on fits to the current LHC Higgs data [9–11,21,22] and on the phenomenological signatures of the heavy Higgs searches [23].

We consider a softly broken Z_2 symmetry in order to suppress the flavor changing neutral current (FCNC) [24]. According to the Z_2 charges of quarks and leptons, there are four types of 2HDMs, Type I, Type II, Type X, and Type Y [25]. Considering the current LHC Higgs data [4,5,22], we accept a simple assumption: the observed 125 GeV state is the light CP -even scalar h^0 in the aligned 2HDM [21]. The exact alignment limit implies that the couplings of h^0 are the same as in the SM. This does not include another interesting possibility that the observed Higgs boson is CP -even H^0 and the light h^0 has been hidden [26]. We note that in the alignment limit the suppressed VV ($V = Z, W$) rate can be naturally explained by H^0, A^0 , or almost degenerate H^0/A^0 . Because of the sum rule of the Higgs couplings to weak gauge bosons, the H^0 - V - V couplings vanish in the exact alignment limit. The CP -odd nature of the pseudoscalar A^0 makes itself a good candidate for the suppressed VV decay. The third case with almost degenerate H^0 and A^0 is motivated by the $\Delta\rho$ constraint [27,28] in the electroweak precision data.

We note that the observed diphoton rate in the heavy Higgs searches at the LHC is a sensitive probe for small $\tan\beta$, where $\tan\beta$ is the ratio of two vacuum expectation values of two Higgs doublets. This is because both the diphoton vertex and the gluon fusion vertex are dominated by the top quark Yukawa coupling which is inversely proportional to $\tan\beta$ in all four types of 2HDM. Small $\tan\beta$ enhances the gluon fusion production cross section as well as the diphoton branching ratio. We study the characteristics of the small $\tan\beta$ region by including higher-order corrections in the gluon fusion production cross section [29], and taking into account the requirements from the perturbativity of the running top quark Yukawa coupling [30], $b \rightarrow s\gamma$ [31], ΔM_{B_d} [32], ϵ_K [33], and R_b [34,35]. We shall revisit each of these constraints and show that if we take a conservative approach the value of $\tan\beta$ can be as low as about 0.5, which is dominantly constrained by the perturbativity. The observed $\gamma\gamma, \tau^+\tau^-$, and $t\bar{t}$ rates put significant new bounds on the $m_{H/A}$ and $\tan\beta$. These are our main results.

The paper is organized in the following way. In Sec. II, we briefly review the aligned 2HDM. Focused on the small $\tan\beta$ region, we thoroughly investigate the low energy constraints in Sec. III. Finally Sec. IV presents our main

results, the excluded regions by the heavy Higgs searches through $\gamma\gamma, \tau^+\tau^-$, and $t\bar{t}$ channels in the aligned 2HDM. Section V contains our conclusions.

II. BRIEF REVIEW OF THE ALIGNED 2HDM

Two Higgs doublet model has two complex Higgs doublet fields, Φ_1 and Φ_2 . Both doublets develop nonzero vacuum expectation values, v_1 and v_2 , which are related with the SM vacuum expectation value through $v = \sqrt{v_1^2 + v_2^2}$. The ratio is $\tan\beta = v_2/v_1$. After the electroweak symmetry breaking, there are five physical degrees of freedom: the light CP -even scalar h^0 , the heavy CP -even scalar H^0 , the CP -odd pseudoscalar A^0 , and two charged Higgs bosons H^\pm . To suppress the unwanted contributions to the FCNC, a discrete Z_2 parity is introduced, under which $\Phi_1 \rightarrow \Phi_1$ and $\Phi_2 \rightarrow -\Phi_2$. If we further assume CP invariance and allow a *soft* Z_2 breaking term, parametrized by m_{12}^2 , in the Higgs potential, the model has seven parameters of $m_h, m_H, m_A, m_{H^\pm}, \tan\beta, \alpha$, and m_{12}^2 . Here α is the mixing angle between h^0 and H^0 . According to the Z_2 charges of the SM fermions, there are four types, Type I, Type II, Type X, and Type Y. The Yukawa couplings in the four types are determined by α and $\tan\beta$ [10].

We adopt a simple but very acceptable assumption that the observed 125 GeV state is h^0 , and its couplings are the same as those of the SM Higgs boson:

$$m_h = 125 \text{ GeV}, \quad \sin(\beta - \alpha) = 1. \quad (1)$$

This is called the alignment limit [21]. An interesting observation is that this limit turns off several Higgs triple vertices. The triple vertices of Higgs bosons with weak gauge bosons or other Higgs bosons can be classified into two categories, one proportional to $\sin(\beta - \alpha)$ and the other proportional to $\cos(\beta - \alpha)$:

$$\begin{aligned} \sin(\beta - \alpha): & \quad g_{hW^+W^-}, \quad g_{hZZ}, \quad g_{ZAh}, \quad g_{W^\pm H^\mp H}, \\ \cos(\beta - \alpha): & \quad g_{HW^+W^-}, \quad g_{HZZ}, \quad g_{ZAh}, \quad g_{W^\pm H^\mp h}, \quad g_{Hhh}. \end{aligned} \quad (2)$$

The couplings proportional to $\cos(\beta - \alpha)$ vanish in the alignment limit.

The exact alignment limit is generically preferred by the current LHC Higgs data including the heavy Higgs boson search results. First it guarantees the SM-like nature of the observed 125 GeV state. The couplings of h^0 with the SM particles are the same as in the SM. Moreover this limit prohibits the dangerous “feed-down” contributions to the observed Higgs rates from the production of heavier Higgs bosons through their decay into h^0 [22,36]. Dominant feed-down sources are $A^0 \rightarrow Zh^0$ and $H^0 \rightarrow h^0 h^0$. Both vertices are proportional to $\cos(\beta - \alpha)$ and thus vanish in the exact

alignment limit. Second, no excess of events in the heavy Higgs searches through the ZZ and WW decay channels can be simply explained: the CP -even H^0 couplings with WW and ZZ vanish in this alignment limit as in Eq. (2); the CP -odd A^0 does not couple with ZZ or WW . In addition, the alignment limit simplifies the phenomenologies of the Higgs sector as the Yukawa couplings of all heavy Higgs bosons are determined by a single parameter $\tan\beta$. We summarize the Yukawa couplings normalized by the SM ones, denoted by $\hat{y}_f^{H,A}$, in Table I. The general expressions are referred to Refs. [10,25].

Focused on the heavy Higgs searches in $\gamma\gamma$, $\tau^+\tau^-$, and $t\bar{t}$ channels, the assumption in Eq. (1) leaves practically the following four parameters:

$$m_H, \quad m_A, \quad m_{H^\pm}, \quad \tan\beta. \quad (3)$$

The soft Z_2 breaking term m_{12}^2 does not affect the heavy Higgs phenomenology considerably. In general m_{12}^2 plays important roles. First it gives more freedom to heavy Higgs boson masses, which is useful to evade FCNC constraints on the charged Higgs boson mass. Second, it affects various Higgs triple couplings. However, the H^0 - h^0 - h^0 vertex, the most relevant Higgs triple coupling in this work, has an overall factor of $\cos(\beta - \alpha)$. m_{12}^2 exerts no influence in the alignment limit.

The heavy Higgs boson masses are indirectly constrained by other low energy data. The $\Delta\rho$ parameter from the electroweak precision measurement is one significant bound. The most up-to-date global fit result of $\Delta\rho$ is [6]

$$\Delta\rho = 0.00040 \pm 0.00024, \quad (4)$$

which has been improved by the observation of the Higgs boson mass. In the 2HDM, not only the heavy neutral Higgs bosons but also the charged Higgs bosons contribute to $\Delta\rho$ radiatively [27,28]. Their new contributions depend only on the heavy Higgs boson masses, not on $\tan\beta$, once $\sin(\beta - \alpha) = 1$ [10].

In Fig. 1, we present the excluded region (yellow colored) in the (m_A, m_H) plane by the $\Delta\rho$ constraint at 95% C.L. We have fixed the charged Higgs boson mass to be $m_{H^\pm} = 350$ GeV as a benchmark point. The shape of the allowed region is the same for different m_{H^\pm} . It is clear that

TABLE I. In the limit of $\sin(\beta - \alpha) = 1$, the Yukawa couplings of H^0 and A^0 with the up-type quarks (u), down-type quarks (d), and the charged lepton (ℓ), normalized by the SM Yukawa coupling $-m_f/v$.

	If $\sin(\beta - \alpha) = 1$			
	Type I	Type II	Type X	Type Y
$\hat{y}_u^H = -\hat{y}_u^A$	$-\frac{1}{\tan\beta}$	$-\frac{1}{\tan\beta}$	$-\frac{1}{\tan\beta}$	$-\frac{1}{\tan\beta}$
$\hat{y}_d^H = \hat{y}_d^A$	$-\frac{1}{\tan\beta}$	$\tan\beta$	$-\frac{1}{\tan\beta}$	$\tan\beta$
$\hat{y}_\ell^H = \hat{y}_\ell^A$	$-\frac{1}{\tan\beta}$	$\tan\beta$	$\tan\beta$	$-\frac{1}{\tan\beta}$

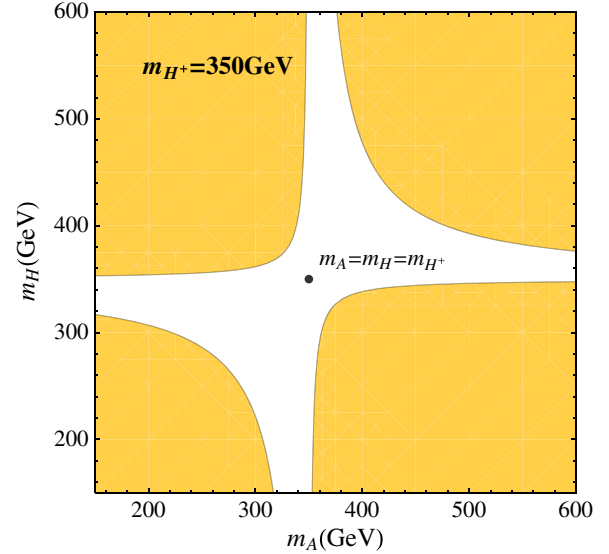


FIG. 1 (color online). The dark (yellow) region is excluded by the $\Delta\rho$ constraint at 95% C.L. when $m_{H^\pm} = 350$ GeV. We set $m_h = 125$ GeV and $\sin(\beta - \alpha) = 1$.

the $\Delta\rho$ constraint can be evaded by mass degeneracy among m_H , m_A , and m_{H^\pm} . If either H^0 or A^0 is degenerate in mass with H^\pm , the new contribution to $\Delta\rho$ vanishes. Another interesting observation is that approximate degeneracy between m_H and m_A also helps to satisfy the $\Delta\rho$ condition unless two masses are very different from m_{H^\pm} .

For the possibility of a gigantic diphoton rate of the heavy Higgs bosons, we first show the branching ratios of H^0 and A^0 into gg and $\gamma\gamma$ for four types of the aligned 2HDM, in Figs. 2 and 3, respectively. For benchmark points, we consider two masses of 200 and 530 GeV. First we note that the $\tan\beta$ dependence of $\text{Br}(H^0 \rightarrow \gamma\gamma)$ is almost the same as that of $\text{Br}(A^0 \rightarrow \gamma\gamma)$ except that the overall values are a little bit higher for A^0 . This is attributed to larger loop function of a pseudoscalar boson for the loop-induced couplings to gg and $\gamma\gamma$ than that of a scalar boson.

In Type I, two branching ratios do not change with $\tan\beta$, for all cases of $m_H = 200, 530$ GeV and $m_A = 200, 530$ GeV. This is because in Type I all of the Yukawa couplings are the same; see Table I. Without the decays into ZZ and WW , all of the decay rates have the same $\tan\beta$ dependence, resulting in constant branching ratios with respect to $\tan\beta$. In Type II, Type X, and Type Y, however, the branching ratios of the decay into gg and $\gamma\gamma$ are maximized for small $\tan\beta$ below about 0.7. This feature is clearly seen in the $m_{H,A} = 200$ GeV case. In the small $\tan\beta$ region, Type II has the largest $\text{Br}(H^0/A^0 \rightarrow gg, \gamma\gamma)$, followed by Type Y, while Types I and X have similar values. In Types II and Y, the b quark Yukawa coupling is proportional to $\tan\beta$, which suppresses the decay into $b\bar{b}$ in small $\tan\beta$ and so enhances the decays into gg and $\gamma\gamma$.

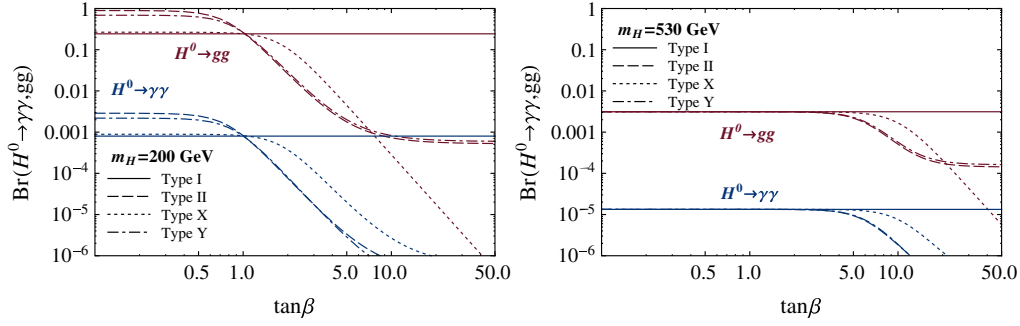


FIG. 2 (color online). Branching ratios of $H^0 \rightarrow \gamma\gamma$ (blue lines) and $H^0 \rightarrow gg$ (red lines) as a function of $\tan\beta$ in four types of 2HDM for $m_H = 200$ GeV and $m_H = 530$ GeV with $\sin(\beta - \alpha) = 1$. Assuming $m_A \approx m_{H^\pm} \gtrsim 600$ GeV, only the decays into the SM particles are considered.

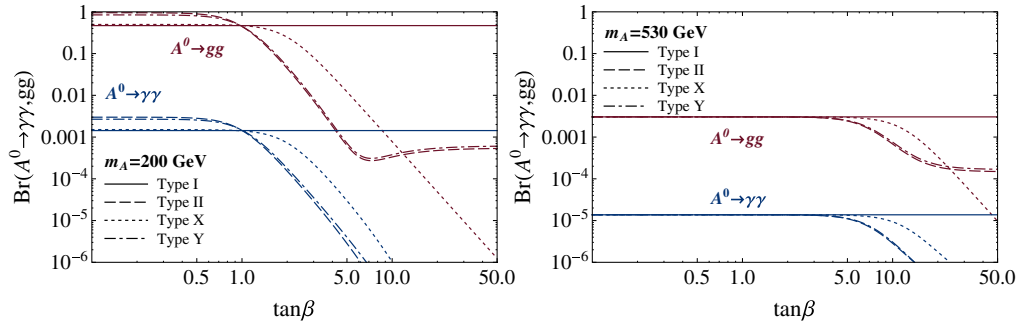


FIG. 3 (color online). Branching ratios of $A^0 \rightarrow \gamma\gamma$ (blue lines) and $A^0 \rightarrow gg$ (red lines) as a function of $\tan\beta$ in four types of 2HDM for $m_A = 200$ GeV and $m_A = 530$ GeV with $\sin(\beta - \alpha) = 1$. Assuming $m_H \approx m_{H^\pm} \gtrsim 600$ GeV, only the decays into the SM particles are considered.

For large $\tan\beta$, other decays into fermion pairs become dominant in Types II, X, and Y; the $b\bar{b}$ mode becomes dominant in Types II and Y. In Type X, the $\tau^+\tau^-$ mode is dominant. It is clear that the diphoton sensitive region is the small $\tan\beta$ region where the gluon fusion production as well as the diphoton decay rate are enhanced.

With the given $\tan\beta = 0.7$, we present the branching ratios into $\tau^+\tau^-$ and $t\bar{t}$ of H^0 and A^0 as a function of $m_{H,A}$ in Fig. 4. Here we assume that H^0 and A^0 decay into the SM particles only. For $m_{H,A} < 2m_t$, the branching ratio into

$\tau^+\tau^-$ is sizeable, of the order of 1 to 10%. In particular, Type Y allows considerably large $\text{Br}(H^0/A^0 \rightarrow \tau^+\tau^-)$ since the τ Yukawa coupling is enhanced in small $\tan\beta$ while the b quark Yukawa coupling is suppressed. On the contrary, Type X has a smaller branching ratio into $\tau^+\tau^-$ as being a few percent. For heavy H^0 and A^0 above the $t\bar{t}$ threshold, the branching ratio into $t\bar{t}$ is so dominant to be practically one in all four types. Therefore, the $t\bar{t}$ resonance search can put a significant bound on the heavy Higgs bosons if $m_{H/A} > 2m_t$, especially in the small $\tan\beta$ region.

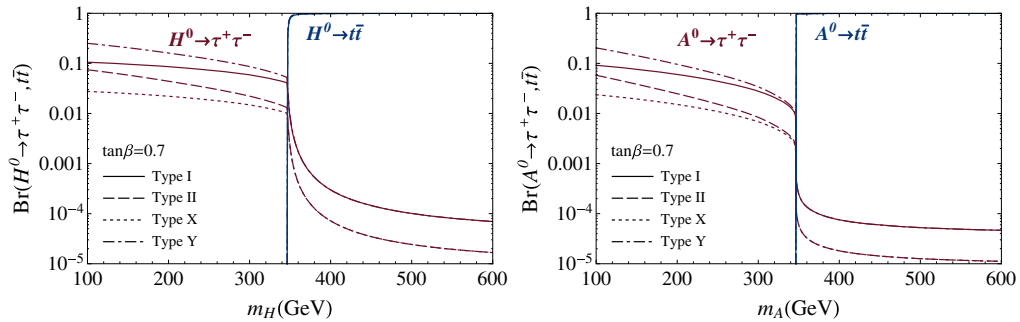


FIG. 4 (color online). For small $\tan\beta = 0.7$ in the alignment limit as $\sin(\beta - \alpha) = 1$, branching ratios of $H^0 \rightarrow \tau^+\tau^-$, $t\bar{t}$ (left) and $A^0 \rightarrow \tau^+\tau^-$, $t\bar{t}$ (right) as a function of $m_{H/A}$ in four types of 2HDM. Only the decays into the SM particles are considered.

Finally we study the $\tan\beta$ dependence of the k -factors in $gg \rightarrow H/A$ productions and $H/A \rightarrow gg$ decays. The k -factor is the ratio of the next-to-leading-order (NLO) or next-to-next-to-leading-order (NNLO) to leading-order (LO) rates. In this work, we calculate the production cross sections and the decay rates at LO by using the parton distribution function of MSTW2008LO [37] and then multiply the k -factor for the gluon-involved production and decays. Other k -factors are relatively small, not affecting the result. The NNLO k -factor for $gg \rightarrow H/A$ production and NLO k -factor for $H/A \rightarrow gg$ decays are calculated by using HIGLU package [38]. The renormalization and factorization scales are fixed to be $\mu_R = \mu_F = \frac{1}{2}m_{H,A}$.

For the given process, the k -factor depends on the heavy Higgs boson mass, the CP property, and the beam energy. The loop-induced processes like $\sigma(gg \rightarrow H/A)$ and $\Gamma(H/A \rightarrow gg)$ have further dependence on $\tan\beta$ because of the different $\tan\beta$ dependence of the t and b quark Yukawa couplings. In the aligned Type I and Type X, however, there is no $\tan\beta$ dependence on the k -factor. Since all of the quark Yukawa couplings with H/A are the same here, the $\tan\beta$ dependence in both LO and NLO rates is the same common factor. When taking the ratio for the k -factor, the $\tan\beta$ dependence is cancelled out. As in the SM, the k -factor of H^0 is 1.9–2.1 for the production at NNLO and 1.4–1.6 for the decay into gg at NLO with a mass range of 100–600 GeV. The k -factor for A^0 production at NNLO is 1.8–2.1 for the same mass range and sharply rises up to 2.4 at the $t\bar{t}$ threshold. The decay k -factor of A^0 at NLO is 1.3–1.7, and it goes up to 2.1 at the $t\bar{t}$ threshold.

In Types II and Y, however, \hat{y}_t and \hat{y}_b have different $\tan\beta$ dependence. The higher-order corrections have different

$\tan\beta$ dependence from the LO, resulting in the $\tan\beta$ dependent k -factors. In Fig. 5 (Fig. 6), we present the k -factors for the gluon fusion production of H^0 (A^0) at NNLO at $\sqrt{s} = 8$ TeV and its decay into gg at NLO in the plane of $(m_{H/A}, \tan\beta)$. The k -factor effect is significant. A common feature is that the k -factor is maximized in the small $\tan\beta$ region and the $t\bar{t}$ threshold. For the gluon fusion production, it can be as large as about 2 for a wide range of the small $\tan\beta$ region and maximally 2.4 for A^0 at the $t\bar{t}$ threshold. The cusps in the plots at the $t\bar{t}$ threshold are due to the appearance of a nonzero imaginary part of the loop function. For the decay into gg , its value is as large as about 1.6 (1.8) for H^0 (A^0) for small $\tan\beta$. Even though the k -factor of decay rate into gg can reduce the branching ratio of diphoton decay, the effect is minor. On the other hand, the large k -factor of gluon fusion production significantly increases the total rate especially for small $\tan\beta$.

III. LOW ENERGY CONSTRAINTS FOR SMALL $\tan\beta$

In the aligned 2HDM, all of the Yukawa couplings depend only on $\tan\beta$. In particular the top quark Yukawa couplings with H/A are inversely proportional to $\tan\beta$ in all four types. A too large top quark Yukawa coupling by small $\tan\beta$ may cause some dangerous problems theoretically and phenomenologically. Theoretically the perturbativity of the top quark Yukawa coupling can be violated, especially when it runs into higher energy. Phenomenologically various low energy observables get affected at the loop level by the charged Higgs boson and the top quark. We consider $b \rightarrow s\gamma$, ΔM_{B_d} , ϵ_K , and R_b . Note that $b \rightarrow s\gamma$ is sensitive to both \hat{y}_t and \hat{y}_b while

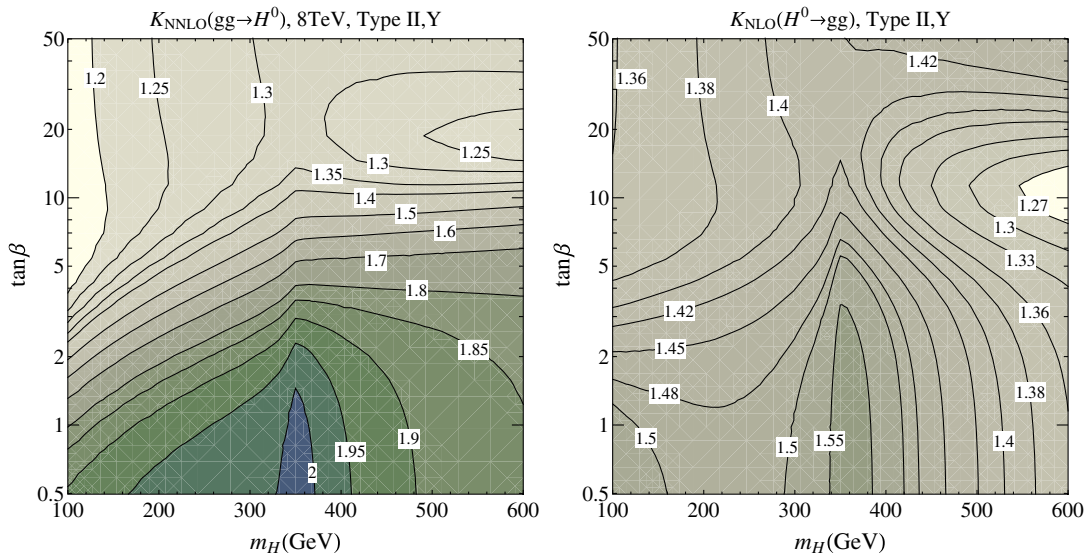


FIG. 5 (color online). NNLO k -factor for $gg \rightarrow H^0$ (left panel) and NLO k -factor for $H^0 \rightarrow gg$ (right panel) for Types II and Y at $\sqrt{s} = 8$ TeV in the $(m_H, \tan\beta)$ plane.

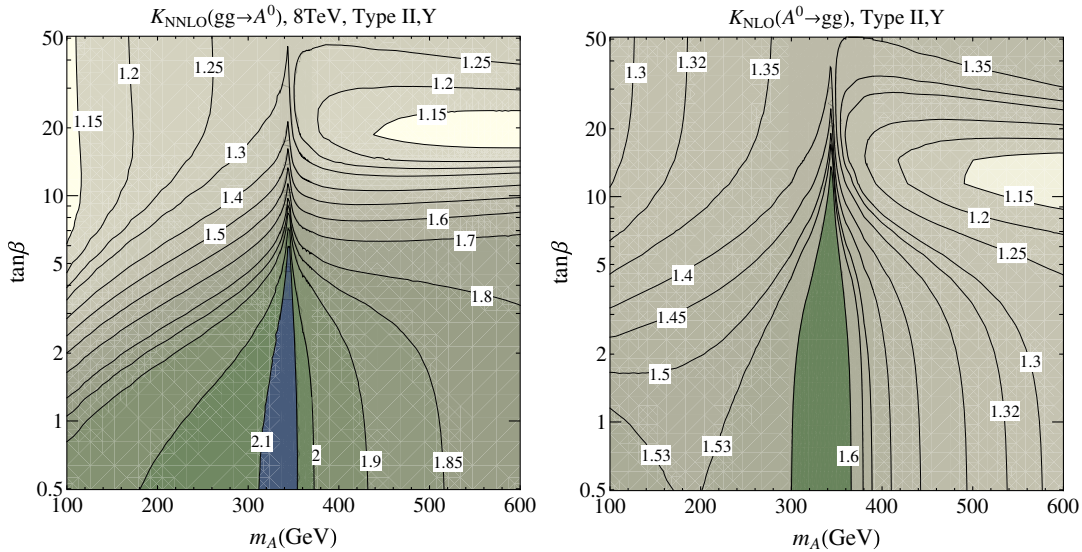


FIG. 6 (color online). NNLO k -factor for $gg \rightarrow A^0$ (left panel) and NLO k -factor for $A^0 \rightarrow gg$ (right panel) for Types II and Y at $\sqrt{s} = 8$ TeV in the $(m_A, \tan\beta)$ plane.

the others are sensitive to \hat{y}_t only [32]. The combined constraints for Type I (X) and Type II (Y) are presented in Fig. 7. The input parameter values and experimental measurements used in this work are summarized in Table II. For the running fermion masses, we refer to Ref. [39].

The enhanced top Yukawa coupling in the small $\tan\beta$ limit can severely threaten the perturbativity of the theory because of the large top quark mass. The problem gets worse if we run the top Yukawa coupling into the higher energy scale since the renormalization group equation of y_t contains a positive y_t^3 term. The large initial value of y_t at the electroweak scale may cause y_t to blow up as the energy scale increases; a Landau pole arises at some high energy scale. In the minimal supersymmetric standard model, for example, the perturbativity of the top Yukawa coupling up to the grand unified theory scale puts a lower bound of $\tan\beta \gtrsim 1.2$ [42]. For the 2HDM, when accepting it as an effective theory with the cutoff scale Λ , we extract the lower bound on $\tan\beta$ by requiring the perturbativity of the top quark Yukawa coupling [30]. For $\Lambda = 10$ TeV (100 TeV), we have $\tan\beta \geq 0.48$ (0.55). We take 0.48 as a low limit of $\tan\beta$ throughout this work.

Various FCNC processes receive additional contributions in the 2HDM through the charged Higgs boson in the loop [31], which significantly constrain the parameter space of the charged Higgs boson mass and $\tan\beta$. We first focus on the $B_d^0 \rightarrow X_s \gamma$ decay which occurs in the SM by the one loop W boson contribution [43]. In the 2HDM, additional contributions are from the charged Higgs boson loop. We adopt the NLO calculation at m_W scale in the 2HDM [44,45], the three-loop anomalous dimension matrix for the renormalization group evolution of Wilson

coefficients from the scale m_W into the scale m_b [46], and finally the two-loop matrix element at m_b [47].¹

For the observed value of $\text{Br}(B_d^0 \rightarrow X_s \gamma)$, we use the averaged value [41] of the measurements by BABAR [51], Belle [52], and CLEO [53]:

$$\text{Br}(B_d^0 \rightarrow X_s \gamma)_{E_\gamma > 1.6 \text{ GeV}}^{\text{exp}} = (3.52 \pm 0.23 \pm 0.09) \times 10^{-4}. \quad (5)$$

Theoretical calculation has many sources of uncertainties such as the renormalization scale, the matching scale, the quark masses, and the Cabibbo-Kobayashi-Maskawa (CKM) matrix element. Dominant uncertainty is in m_c/m_b . The observed rate of $\text{Br}(B_d^0 \rightarrow X_c e \bar{\nu}_e)$, which is used for the normalization of $\text{Br}(B_d^0 \rightarrow X_s \gamma)$ in order to cancel the large theoretical uncertainties from m_b^5 and the CKM factor, also has large uncertainty. The total uncertainty is crucial when comparing the theoretical prediction and the observation. Two different error analysis methods have been discussed [44], the Gaussian method and the scanning method. In the Gaussian method, the final theoretical error of $\text{Br}(B_d^0 \rightarrow X_s \gamma)$ is the quadrature sum of all the errors, yielding the total uncertainty as $\pm 9\%$. In the scanning method, we vary all the input parameters independently within the 1σ range and calculate $\text{Br}(B_d^0 \rightarrow X_s \gamma)$. Its maximum and minimum values give the final error, which is $-21\% \sim +25\%$ [44].

In Fig. 7, we present the exclusion regions of the parameter space of $(m_{H^\pm}, \tan\beta)$ at 95% C.L. in Types I and X (left) and Types II and Y (right) by using the

¹There are full NNLO calculations within the SM [48,49] and three-loop NNLO Wilson coefficients at electroweak scale within the 2HDM [50].

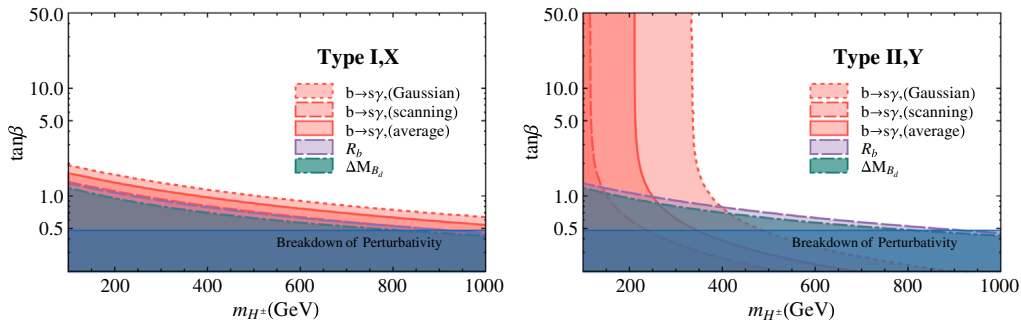


FIG. 7 (color online). Combined exclusion plot at 95% C.L. in $(m_{H^\pm}, \tan\beta)$ plane from $b \rightarrow s\gamma$, R_b , ΔM_{B_d} , and the perturbativity of the top Yukawa coupling at 10 TeV. See the main text regarding the *Gaussian* and *scanning* methods for the error analysis of $B_d \rightarrow X_s\gamma$ theory prediction.

Gaussian method (dashed) and the scanning method (dotted). Since there is no leptonic contribution, the excluded region for Type I (Type II) is equivalent for Type X (Type Y). We also note that the new contributions have two dominant terms, one with a \hat{y}_t^2 factor and the other with a $\hat{y}_t\hat{y}_b$ factor. It should be emphasized that the term with $\hat{y}_t\hat{y}_b$ has no m_b/m_t suppression relative to the term with \hat{y}_t^2 since the latter also receives the m_b factor from the mass insertion in the $b \rightarrow s\gamma$ dimension-5 effective operator.

In Types I and X, two contributions from the \hat{y}_t^2 term and the $\hat{y}_t\hat{y}_b$ term have common factor $(1/\tan\beta)^2$. Therefore, $\text{Br}(B_d^0 \rightarrow X_s\gamma)$ constrains only the small $\tan\beta$ region. The charged Higgs boson mass is not bounded. And two different error analysis methods yield similar results: for $m_{H^\pm} = 1$ TeV, $\tan\beta \geq 0.63$ for the Gaussian method, and $\tan\beta \geq 0.45$ for the scanning method.

In Types II and Y, the $\text{Br}(B_d^0 \rightarrow X_s\gamma)$ constraints on $\tan\beta$ for the heavy charged Higgs boson are weaker than in Types I and X, as shown in Fig. 7. If the constraints from the perturbativity of the top quark Yukawa coupling are included, the lower bound on $\tan\beta$ for the heavy charged Higgs boson is similar in all four types. However, the $\text{Br}(B_d^0 \rightarrow X_s\gamma)$ constraints exclude a light H^\pm in Types II and Y regardless of the $\tan\beta$ value. This is because the contribution from the $\hat{y}_t\hat{y}_b$ term is constant with respect to $\tan\beta$ in Types II and Y. It is notable that the lower bounds

on m_{H^\pm} are seriously different according to the error analysis method.

With the Gaussian method, we have $m_{H^\pm} \gtrsim 330$ GeV, and with the scanning method, $m_{H^\pm} \gtrsim 110$ GeV. The two error analysis methods can be regarded as two extreme cases in dealing with correlations among individual errors. In the remaining analysis, we take the average value of the two errors and get the bounds on $\tan\beta$ and m_{H^\pm} , as in Refs. [25,32].

To understand this large difference, we show the branching ratio $\text{Br}(B_d^0 \rightarrow X_s\gamma)$ in Types II and Y as a function of m_{H^\pm} in Fig. 8 for $\tan\beta = 5$. The solid band represents the 2σ allowed region of the current experimental data, and the dashed (dotted) band is that of the theoretical calculation at NLO with the scanning (Gaussian) method. When the difference between two central values of the experimental data and the theoretical calculation exceeds the quadrature sum of two errors for the given m_{H^\pm} , we exclude the m_{H^\pm} . Since the decreasing slope of theory prediction with respect to m_{H^\pm} is very gentle especially around the intersection between theory and experiment, the lower limit of m_{H^\pm} is highly sensitive to either theory prediction or experimental measurement. The 10% difference between the two theory errors causes a roughly 200 GeV difference of the m_{H^\pm} lower bound. Care should be taken when one treats the lower bound on m_{H^\pm} . Another sensitive control is the adoption of the photon energy cut, $E_\gamma > 1.6$ GeV, in

TABLE II. Summary of input parameters and experimental measurements of low energy physics. See the text for the details of the parameter values of the CKM matrix.

Parameters	Value	Parameters/Measurements	Value
$\alpha_e(Q^2 = m_W^2)$	1/128	$\bar{\rho}$	$0.147^{+0.069}_{-0.067}$
$\alpha_s(m_Z)$	0.118	$\bar{\eta}$	$0.329^{+0.050}_{-0.039}$
m_h	125.7 ± 0.4 GeV [6]	A	0.810 ± 0.026
m_t	173.2 ± 0.9 GeV [6]	λ	0.225
$m_b(m_b)$	4.18 ± 0.03 GeV [6]	$\text{Br}(B_d^0 \rightarrow X_c e \bar{\nu}_e)$	$(10.1 \pm 0.4) \times 10^{-2}$ [6]
$m_c(m_c)$	1.275 ± 0.025 GeV [6]	$\text{Br}(B_d^0 \rightarrow X_s\gamma)_{E_\gamma > 1.6 \text{ GeV}}$	$(3.52 \pm 0.23 \pm 0.09) \times 10^{-4}$ [41]
m_τ	1.78 GeV [6]	ΔM_{B_d}	0.507 ± 0.004 [41]
$f_{B_d} B_{B_d}^{1/2}$	216 ± 15 MeV [40]	R_b	0.21629 ± 0.00066 [34]

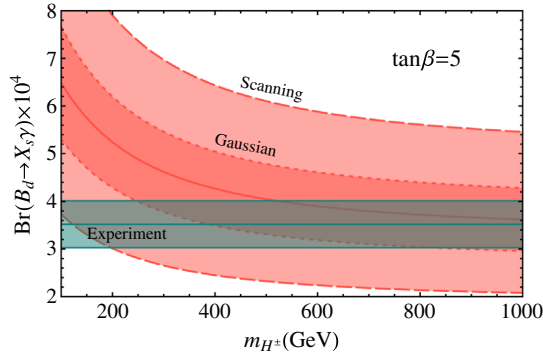


FIG. 8 (color online). Branching ratio of $B_d \rightarrow X_s \gamma$ with 2σ error range in the Types II and Y 2HDM at NLO QCD with respect to m_{H^\pm} . We choose $\tan\beta = 5$.

the experimental measurement. We set $\delta = 0.33$ where $E_\gamma^{\text{cut}} = (1 - \delta)m_b/2$. The branching ratio is reduced by 10% after applying the E_γ cut, yielding a smaller value for the lower bound on m_{H^\pm} .

Finally we mention that the lower bound on m_{H^\pm} including the NNLO Wilson coefficient of 2HDM was reported as $m_{H^\pm} > 380$ GeV for Types II and Y in Ref. [50] where the authors adopt Gaussian method for the error analysis. Comparing with our result $m_{H^\pm} > 330$ GeV for the Gaussian error analysis, the difference is acceptable when considering the sensitivity of the m_{H^\pm} lower bound as we discussed before. Nevertheless this difference in m_{H^\pm} does not change our main results.

We now move on to the ΔM_{B_d} constraint. The current experimental value is [41]

$$\Delta M_{B_d}^{\text{exp}} = 0.507 \pm 0.004. \quad (6)$$

ΔM_{B_d} is induced by $B_d^0 - \bar{B}_d^0$ mixing to which the charged Higgs boson loop can contribute significantly in the 2HDM. Even though both top quark Yukawa coupling and b quark Yukawa coupling are involved in the H^\pm loop, the y_b contribution is suppressed by m_b^2/m_t^2 . Only the y_t contribution becomes relevant, which is proportional to $(1/\tan\beta)^4$ in all types. Too small $\tan\beta$ is excluded. The usual conclusion is that ΔM_{B_d} puts on a lower bound as $\tan\beta \gtrsim 1$ for $m_{H^\pm} = 500$ GeV.

We reexamine the ΔM_{B_d} constraint to which the LO contribution² in the 2HDM is

$$\Delta M_{B_d} = \frac{G_F^2}{6\pi^2} |V_{td}^* V_{tb}|^2 f_{B_d}^2 B_{B_d} m_{B_d} \eta_b m_W^2 S_{2\text{HDM}}(x_W, x_H). \quad (7)$$

²Although the NLO QCD correction within the 2HDM has been studied in Ref. [54], non-negligible inconsistencies are reported in Ref. [55].

Here we use the long-distance quantity $f_{B_d} B_{B_d}^{1/2} = 216 \pm 15$ MeV [40] and the short-distance QCD contribution $\eta_b = 0.552$ [56]. The expressions for the 2HDM Inami-Lim functions $S_{2\text{HDM}}$ are referred to in Ref. [57]. The constraint from the observed ΔM_{B_d} on the 2HDM, i.e., $S_{2\text{HDM}}$, is possible only when the other parameters in the right-hand side of Eq. (7) are known. However, the usually quoted value of $|V_{td}| = (8.4 \pm 0.6) \times 10^{-3}$ [6] is based on the ΔM_{B_d} measurement itself. In the 2HDM, we need other independent measurements of V_{td} . The CKM factor $|V_{td}^* V_{tb}|^2$ is represented in the Wolfenstein parametrization as

$$|V_{td}^* V_{tb}|^2 = A^2 \lambda^6 |1 - \bar{\rho} + i\bar{\eta}|^2. \quad (8)$$

Fixing four parameters of A , λ , $\bar{\rho}$, and $\bar{\eta}$ independently of ΔM_{B_d} will determine the CKM factor. First $\lambda = 0.225$ is measured very precisely from $K \rightarrow \pi \ell \nu$ decays. The semileptonic $\bar{B} \rightarrow D^{(*)} \ell \bar{\nu}$ ($\ell = e, \mu$) decays leads to $|V_{cb}| = (41.1 \pm 1.3) \times 10^{-3}$ [6], which in turn determines A via $|V_{cb}| = A\lambda^2$: $A = 0.810 \pm 0.026$.

The $(\bar{\rho}, \bar{\eta})$ is the position of the apex of the CKM unitary triangle. We emphasize that the global fit for $(\bar{\rho}, \bar{\eta})$ will be significantly affected by 2HDM contributions. The SM fit results are not appropriate here. Using tree-dominant processes is the only way to obtain $(\bar{\rho}, \bar{\eta})$ properly. We take $|V_{ub}|$ measurement from the semileptonic $\bar{B} \rightarrow \pi \ell \bar{\nu}$ decays and the CKM angle $\gamma(\phi_3)$ measurement from $B \rightarrow DK$ decays, which yield [58]

$$\bar{\rho} = 0.147_{-0.067}^{+0.069}, \quad \bar{\eta} = 0.329_{-0.039}^{+0.050}. \quad (9)$$

Finally the CKM factor in Eq. (7) becomes

$$|V_{td}^* V_{tb}|^2 = (7.2 \pm 1.1) \times 10^{-5}, \quad (10)$$

of which the central value as well as the uncertainty are significantly different from those based on the ΔM_{B_d} in the SM. In Fig. 7, we present the excluded region by ΔM_{B_d} at 95% C.L. The bound is rather weak: $\tan\beta \gtrsim 1.1$ even for a light charged Higgs boson with $m_{H^\pm} = 150$ GeV. The constraint from ε_K , the time-dependent CP violation of the K meson, leads to a similar result [33], which is not very meaningful due to the large theoretical uncertainty from the CKM factor. We do not show this result.

We finally study the constraint from $Z \rightarrow b\bar{b}$ process. Its relative contribution to the Z hadronic width is parametrized by R_b , which is very precisely measured as [34]

$$R_b^{\text{exp}} = 0.21629 \pm 0.00066. \quad (11)$$

In the 2HDM, R_b is also modified through the top quark and charged Higgs loop. Although both t and b quark Yukawa couplings are involved, the b quark contribution is suppressed by m_b^2/m_W^2 . In Fig. 7, we present the exclusion region by R_b (violet) at 95% C.L. The constraints are

almost the same for all types of 2HDM. In Type I, it is very similar to the excluded region by $b \rightarrow s\gamma$ with the scanning error analysis. Type II is more affected by R_b , especially for small $\tan\beta$ and large m_{H^\pm} .

IV. CONSTRAINTS FROM THE HEAVY HIGGS SEARCH

The heavy Higgs boson search at the LHC has been performed through various decay channels. No significant excess in the $ZZ \rightarrow 2\ell 2\nu$ mode puts the most stringent bound on the heavy Higgs boson mass, if the heavy state is a SM-like Higgs boson: $M_H \gtrsim 580$ GeV [12,13]. The channel of $H \rightarrow WW \rightarrow \ell\nu\ell\nu$ has been searched for mass above 260 GeV but has not reached the sensitivity yet for the SM-like heavy Higgs boson [14]. In the fermionic decay channels, the dijet resonance searches are available only for a very heavy state like $m_{jj} \gtrsim 800$ GeV, because of huge QCD backgrounds [15]. On the other hand, the $t\bar{t}$ resonance search covers much a lower mass region from 500 GeV [17]. Remarkable performance is from the $\tau^+\tau^-$ mode [16] which probes 100–1000 GeV region by using τ reconstruction and identification algorithms [59].

Nevertheless the diphoton mode, if large enough to observe, is also very efficient for the heavy Higgs boson search especially in the aligned 2HDM. The Landau–Yang theorem excludes the possibility of the spin-1 state [60]. The observed suppression of the coupling with ZZ disfavors the massive graviton hypothesis, of which the interaction is through the energy-momentum tensor. In addition, the diphoton mode probes, although indirectly, all of the Yukawa couplings through the fermions in the loop. Its correlation with other heavy Higgs searches through $\tau^+\tau^-$ and $t\bar{t}$ can be very significant.

Recently the ATLAS collaboration reported the search for the diphoton resonances in a considerably wider mass range than previous searches, 65–600 GeV at $\sqrt{s} = 8$ TeV [18], and the CMS reported the 150–850 GeV range [19]. There are a few excesses with a 2σ local significance. A worthwhile question is whether any of these is consistent with other heavy Higgs searches. The signal rates observed by the ATLAS are

$$\sigma^{8 \text{ TeV}}(pp \rightarrow \mathcal{H} \rightarrow \gamma\gamma) \approx \begin{cases} 7.6_{-2.9}^{+1.8} \text{ fb} & \text{for } m_{\gamma\gamma} = 200 \text{ GeV}; \\ 1.4_{-0.4}^{+0.3} \text{ fb} & \text{for } m_{\gamma\gamma} = 530 \text{ GeV}. \end{cases} \quad (12)$$

The small $\tan\beta$ region of the aligned 2HDM, where both the gluon fusion production and the diphoton decay are enhanced, is constrained significantly.

In comparing the 2HDM contributions with the observed upper limits, the commonly calculated $\sigma \cdot \text{Br}$ is not relevant when the resonance is not narrow. The experimental criteria for a narrow resonance is that the total width be smaller than $0.09 \text{ GeV} + 0.01m_{H,A}$ [18]. The total widths of both

H^0 and A^0 exceed this criteria in the parameter region of $m_{H,A} > 2m_t$ and small $\tan\beta$ for all types and additionally in large $\tan\beta$ for Type II and Type Y. Finite width effects are usually implemented with a Breit–Wigner distribution. The larger the total width is, the smaller the peak rate is. We note that the magnitude of the peak rate depends crucially on the bin size. A smaller bin suppresses the peak rate more. For example, the diphoton rate for $m_A = 530$ GeV and $\tan\beta = 0.7$ is reduced into about 15% (76%) of that in the narrow width approximation for the $m_{\gamma\gamma}$ bin size 10 GeV (100 GeV). Based on the experimental results, we adopt the 5 GeV bin size for diphoton [4,5] and $\tau^+\tau^-$ modes [16] but the 100 GeV bin size for the $t\bar{t}$ mode [17].

There are two candidates in the aligned 2HDM for a large diphoton rate but suppressed VV rate, H^0 and A^0 . In what follows, we consider three cases: (i) $m_H \lesssim 600$ GeV while $m_A \approx m_{H^\pm} \gtrsim 600$ GeV; (ii) $m_A \lesssim 600$ GeV while $m_H \approx m_{H^\pm} \gtrsim 600$ GeV; and (iii) $m_H \approx m_A \approx m_{H^\pm} \lesssim 600$ GeV.

A. $m_H \lesssim 600$ GeV

In the aligned 2HDM, the sum rule of the Higgs bosons with weak gauge bosons results in $g_{HVV} = 0$; the heavy CP -even Higgs boson H^0 is a natural candidate for the not-so-heavy scalar which does not decay into WW/ZZ . We assume that A^0 and H^\pm are almost degenerate and much heavier than H^0 . The degeneracy satisfies the $\Delta\rho$ condition, and the heavy H^\pm relaxes the FCNC constraints. Since the bound from the perturbativity of the running top Yukawa coupling is not affected by m_A nor m_{H^\pm} , it becomes the most important one; see Fig. 7.

In Fig. 9, we present the excluded regions from the heavy Higgs searches through $\gamma\gamma$ (orange), $\tau^+\tau^-$ (green), and $t\bar{t}$ (red). The blue region is where the perturbativity of the running top quark Yukawa coupling is broken at 10 TeV. For all four types, the data on the heavy Higgs search put on significant *new* bounds. In Type I, all three modes put bounds on small $\tan\beta$ because all of the Yukawa couplings are inversely proportional to $\tan\beta$. The $\tau^+\tau^-$ mode excludes $\tan\beta \lesssim 0.8$ for $m_H \lesssim 340$ GeV. The diphoton rates put on a meaningful new constraint for $m_H \lesssim 350$ GeV. Since both amplitudes for $gg \rightarrow H^0$ and $H^0 \rightarrow \gamma\gamma$ develop a maximum at the $t\bar{t}$ threshold, a strong bound of $\tan\beta \gtrsim 1.2$ applies for $m_H \approx 2m_t$. Neither $\tau^+\tau^-$ nor $\gamma\gamma$ mode constrains the mass region above $2m_t$. This is partially because a newly opened $t\bar{t}$ decay mode is dominant, which reduces the branching ratio of $H^0 \rightarrow \gamma\gamma, \tau^+\tau^-$. The increase in the total width weakens the constraint further because of the finite width effect. Finally the $t\bar{t}$ data, which are available for $m_{t\bar{t}} > 500$ GeV, exclude the small $\tan\beta$ region below 0.6–0.7. This is the only bound for $m_H \gtrsim 500$ GeV.

In Type II, the $\tau^+\tau^-$ mode excludes the large $\tan\beta$ region where both \hat{y}_b and \hat{y}_τ are proportional to $\tan\beta$. The gluon

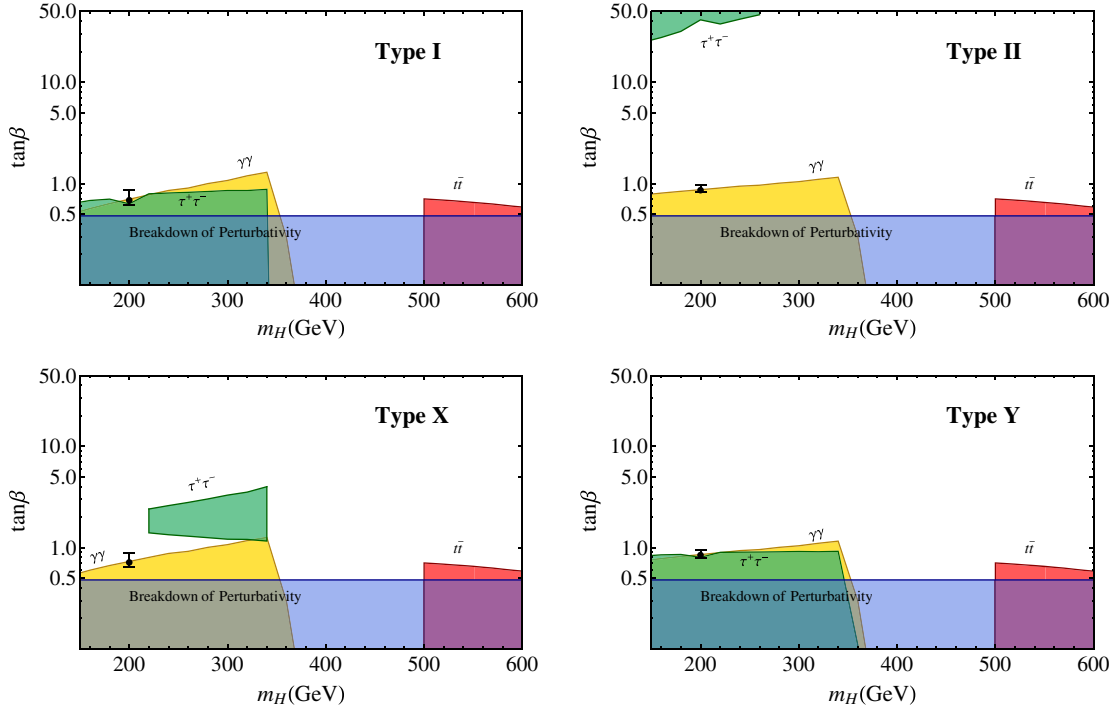


FIG. 9 (color online). For $m_H \lesssim 600$ GeV while $m_A \simeq m_{H^\pm} \gtrsim 600$ GeV in the aligned 2HDM, the combined exclusion plot at 95% C.L. from heavy Higgs searches (through $\gamma\gamma$, $\tau^+\tau^-$, and $t\bar{t}$) and the breakdown of perturbativity of top Yukawa coupling at 10 TeV. The diphoton resonance at 200 GeV with 2σ local significance observed by ATLAS [18] is presented for reference.

fusion production is enhanced by large \hat{y}_b , and the decay rate is additionally enhanced by large \hat{y}_τ . This gives quite a strong bound on $\tan\beta$ especially for light H^0 : if $m_H \simeq 150$ GeV, for example, $\tan\beta$ should be less than about 25. The diphoton constraint is stronger than in Type I, especially for $m_H \simeq 150$ –200 GeV. This is because both $\text{Br}(H^0 \rightarrow gg)$ and $\text{Br}(H^0 \rightarrow \gamma\gamma)$ are larger than in Type I for $\tan\beta \lesssim 1$; see Fig. 2. The $t\bar{t}$ constraint is almost the same as in Type I, $\tan\beta \gtrsim 0.7$ for $m_H \simeq 500$ –600 GeV.

In Type X, the constraints from the $\gamma\gamma$ and $t\bar{t}$ modes are almost the same as in Type I. One exception is the $\tau^+\tau^-$ exclusion region, which has a shape of island around $\tan\beta \sim 2$ for $m_H \simeq 220$ –340 GeV. This is because in Type X the increasing rate of $\text{Br}(H^0 \rightarrow \tau^+\tau^-)$ with $\tan\beta$ is more rapid than the decreasing rate of gluon fusion production of H^0 up to $\tan\beta \simeq 2$. For $\tan\beta \gtrsim 2$, $\text{Br}(H^0 \rightarrow \tau^+\tau^-)$ converges while the production rate continues to decrease. So, the rate $\sigma(gg \rightarrow H^0) \cdot \text{Br}(H^0 \rightarrow \tau^+\tau^-)$ is maximized around $\tan\beta \sim 2$. In Type Y where $\hat{y}_\tau = 1/\tan\beta$, the constraints from $\gamma\gamma$ and $t\bar{t}$ are very similar to those in Type I. The $\tau^+\tau^-$ constraint excludes the small $\tan\beta$ region.

For a reference, we present in Fig. 9 the parameter ranges which can explain a diphoton excess with a 2σ local significance in Eq. (12). The black blob explains the central value in Eq. (12), and the error bar is for 2σ . The one at $m_{\gamma\gamma} = 530$ GeV is absent, because $\text{Br}(H^0 \rightarrow \gamma\gamma)$ itself

is too small. The $m_{\gamma\gamma} = 200$ GeV resonance can be accommodated in all four types³ if $\tan\beta \simeq 0.7$ –0.8. And the $\tau^+\tau^-$ mode starts to exclude the resonance in Type I and Type Y.

B. $m_A \lesssim 600$ GeV

We consider the cases where the A^0 mass is not so heavy while H^0 and H^\pm are degenerate to each other and heavy enough to evade FCNC constraints. Figure 10 shows the exclusion plot based on various heavy Higgs search and perturbativity. The overall behavior of the exclusion region is similar to that of the $m_H \lesssim 600$ GeV case. But the area is considerably larger than the $m_H \lesssim 600$ GeV case. It is because the loop function for the g - g - A^0 vertex is larger than that for the g - g - H^0 vertex.

The $\gamma\gamma$ data exclude the small $\tan\beta$ region for $m_A \lesssim 350$ GeV in all four types, maximally at the $t\bar{t}$ threshold. The lower bound on $\tan\beta$ for $m_A = 340$ GeV is about 3 for Type I and about 2 for other types. The $\tau^+\tau^-$ data exclude the small $\tan\beta$ regions for Types I and Y, but the bound is weaker than that from $\gamma\gamma$. In Type II, a new island-shaped exclusion region by the $\tau^+\tau^-$ mode appears around $\tan\beta \sim 1$. The origin of the excluded region is similar to the case of Type X, i.e., the maximized rate of $\sigma(gg \rightarrow H^0) \cdot$

³Since the $m_{\gamma\gamma} = 200$ GeV resonance is at a 2σ local significance, it is located at the boundary of the $\gamma\gamma$ exclusion region at 95% C.L.

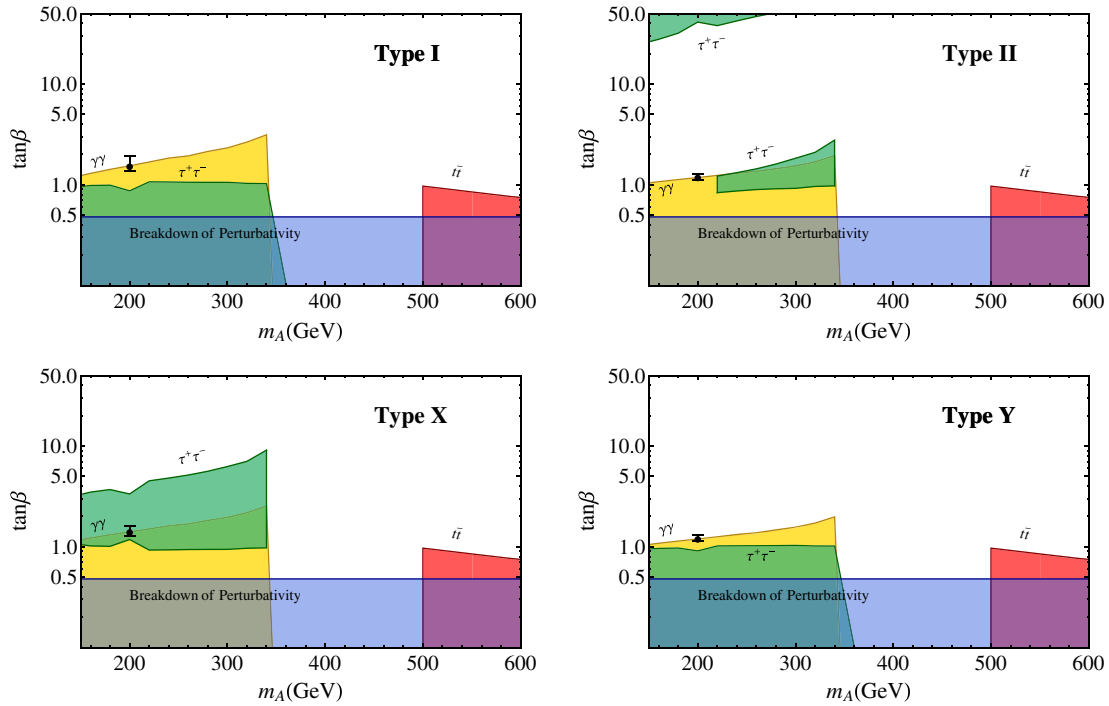


FIG. 10 (color online). For $m_A \lesssim 600$ GeV while $m_H \approx m_{H^\pm} \gtrsim 600$ GeV in the aligned 2HDM, the combined exclusion plot at 95% C.L. from the heavy Higgs searches (through $\gamma\gamma$, $\tau^+\tau^-$, and $t\bar{t}$) and the perturbativity of the top quark Yukawa coupling at 10 TeV. The diphoton excess at 200 GeV with a 2σ local significance observed by ATLAS [18] is presented for reference.

$\text{Br}(H^0 \rightarrow \tau^+\tau^-)$ at $\tan\beta \sim 1$. The enhanced gluon fusion production rate for A^0 yields this additional island exclusion region for Type II. For $m_A \approx 340$ GeV we have $\tan\beta > 3$. Unexpectedly large is the $\tau^+\tau^-$ exclusion region in Type X. It covers the region for $m_A \approx 150\text{--}340$ GeV and $\tan\beta \approx 1.0\text{--}9.0$. Particularly at the $t\bar{t}$ threshold, we have the condition $\tan\beta > 9$, which is the strongest bound ever. Finally the $t\bar{t}$ constraints are similar to the $m_H \lesssim 600$ GeV case: $\tan\beta \gtrsim 0.9$ for $m_A \sim 500$ GeV.

For reference we show the parameter regions for possible diphoton resonances. The $m_{\gamma\gamma} = 200$ GeV resonance can be explained by a rather moderate value of $\tan\beta \sim 1$. It is very interesting that in Type X the $\tau^+\tau^-$ constraint excludes the $m_{\gamma\gamma} = 200$ GeV resonance. If the resonance were real, we should have seen another resonance in the $\tau^+\tau^-$ mode for Type X. The $m_{\gamma\gamma} = 530$ GeV resonance is not explained by A^0 ; $\text{Br}(A^0 \rightarrow \gamma\gamma)$ is too small.

C. $m_H \simeq m_A \sim m_{H^\pm} \lesssim 600$ GeV

The final scenario is that H^0 and A^0 are almost degenerate and within the current LHC reach. This degeneracy is not artificial but natural in many new physics models such as the minimal supersymmetric standard model. One crucial constraint is from $\Delta\rho$ in electroweak precision data, as discussed in Sec. II. The charged Higgs boson mass is not free anymore, which brings additional constraints from various flavor physics data. Particularly in

Type II and Y, the combination of the lower bound on m_{H^\pm} from $b \rightarrow s\gamma$ with the $\Delta\rho$ puts additional lower bounds on $m_{H,A}$. We include all of the low energy constraints comprehensively and present the combined exclusion region in Fig. 11. Other heavy Higgs search bounds from the $\gamma\gamma$, $\tau^+\tau^-$, and $t\bar{t}$ data as well as the breakdown of the perturbativity of the top Yukawa coupling at $\Lambda = 10$ TeV are also shown.

The combined contributions from H^0 and A^0 enhance the rate of all heavy Higgs search modes and expand the exclusion regions. The overall shapes are similar to two single resonance cases: the $\gamma\gamma$ mode excludes small $\tan\beta$ region for $m_{H,A} \lesssim 340$ GeV; the $\tau^+\tau^-$ mode excludes small $\tan\beta$ for Types I and Y, the island region around $\tan\beta \sim \mathcal{O}(1)$ for Types II and X, and additional large $\tan\beta$ for Type II; the $t\bar{t}$ mode excludes small $\tan\beta$ for $m_{H,A} \gtrsim 500$ GeV. For reference, we present the parameter region for two diphoton resonances. The $m_{\gamma\gamma} = 200$ GeV resonance is well explained with a moderate value of $\tan\beta \approx 1.3$ in all four types. However, in Type X, the $\tau^+\tau^-$ constraint excludes this resonance. Even with double contributions from H^0 and A^0 , the $m_{\gamma\gamma} = 530$ GeV resonance cannot be explained in the aligned 2HDM. If the total width is very narrow, the extreme value of $\tan\beta \approx 0.1$ may explain the excess at $m_{\gamma\gamma} = 530$ GeV. However, this is not realistic at all; the finite width effects reduce the diphoton rate too much. More importantly, the $t\bar{t}$ constraint excludes this small $\tan\beta$ region completely. In summary,

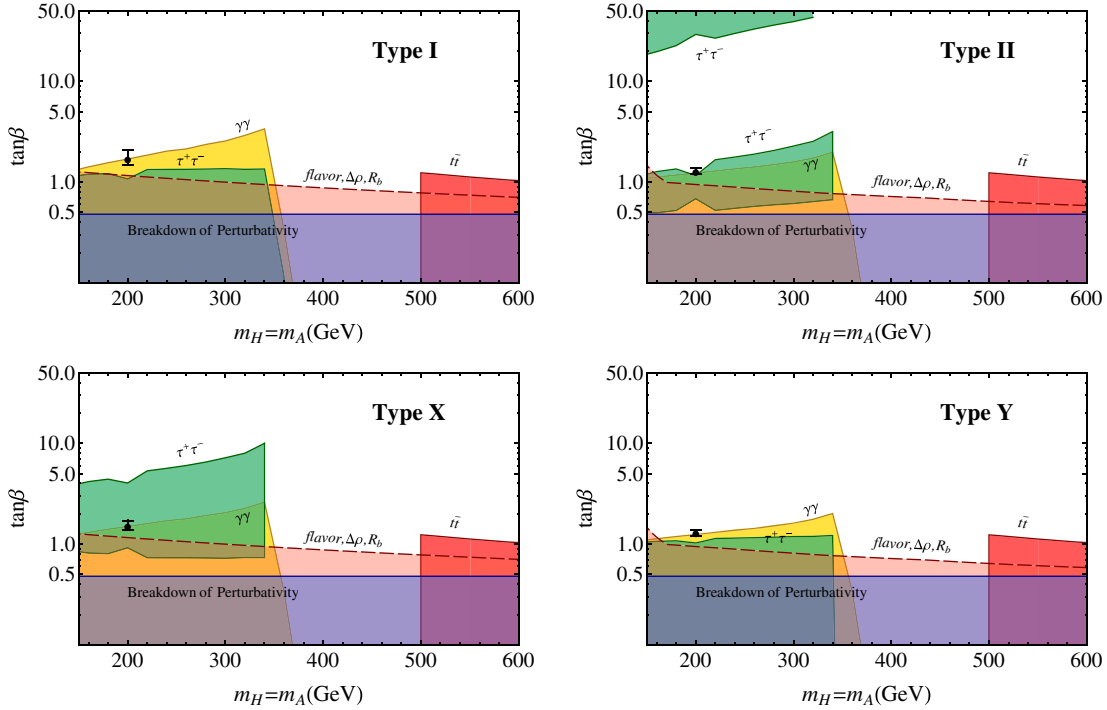


FIG. 11 (color online). For $m_H \approx m_A \sim m_{H^\pm} \lesssim 600$ GeV in the aligned 2HDM, the combined exclusion plot at 95% C.L. from heavy Higgs searches (through $\gamma\gamma$, $\tau^+\tau^-$, and $t\bar{t}$) flavor physics, $\Delta\rho$, R_b , and the breakdown of perturbativity of top Yukawa coupling at 10 TeV. The diphoton resonance at 200 GeV with 2σ local significance observed by ATLAS [18] is presented for reference.

the aligned 2HDM cannot accommodate the $m_{\gamma\gamma} = 530$ GeV resonance.

V. CONCLUSIONS

We studied the constraints from the current LHC heavy neutral Higgs boson searches at $\sqrt{s} = 8$ TeV in four types of the 2HDM with a softly broken Z_2 symmetry. Considering the observation of the very SM-like 125 GeV state and the nonobservation of the ZZ decay mode of the heavy Higgs boson, we took the alignment limit. The observed new particle is the light CP -even Higgs boson h^0 with the same couplings as in the SM. Then the target of the heavy neutral Higgs search in the aligned 2HDM is H^0 , A^0 , or degenerate H^0/A^0 .

Special attention was paid in the small $\tan\beta$ region which is sensitive to the diphoton mode. In all of the four types of 2HDM, small $\tan\beta$ resulted in the enhancement of gluon fusion production and diphoton branching ratios. Moreover the k -factor was enhanced for small $\tan\beta$ in Type II and Type Y. We reinvestigated the indirect constraints from $b \rightarrow s\gamma$, ΔM_{B_d} , R_b , and ϵ_K . We found that the constraints from $b \rightarrow s\gamma$ and ΔM_{B_d} can be weaker. For $b \rightarrow s\gamma$, a different error analysis method seriously changed the lower bounds on $\tan\beta$ and m_{H^\pm} in Types II and Y. The constraint from ΔM_{B_d} was shown to be weak if the involved CKM factor was deduced from tree dominant processes. R_b and ϵ_K constraints were similar, leading to $\tan\beta > 0.5$ for

$m_{H^\pm} \approx 800$ GeV. As a theoretical constraint, the perturbativity of the running top Yukawa coupling was also studied. With the cutoff scale 10 TeV, the perturbativity was broken if $\tan\beta \lesssim 0.5$.

The heavy neutral Higgs boson search data from $\gamma\gamma$, $\tau^+\tau^-$, and $t\bar{t}$ modes were used to constrain the aligned 2HDM. With two candidates of H^0 and A^0 , we considered three cases, (i) $m_H \lesssim 600$ GeV, (ii) $m_A \lesssim 600$ GeV, and (iii) $m_H \approx m_A \sim m_{H^\pm} \lesssim 600$ GeV. All of them had very similar shapes and the location of the exclusion region from $\gamma\gamma$, $\tau^+\tau^-$, and $t\bar{t}$ data. The difference was the area. Since the g - g - A^0 vertex had much larger loop function than g - g - H^0 , the case (iii) had the strongest constraints from the heavy Higgs search. The diphoton resonance search data excluded the small $\tan\beta$ region for $m_{H,A} \lesssim 340$ GeV in all four types. The $\tau^+\tau^-$ mode excluded small $\tan\beta$ for Types I and Y, an island region around $\tan\beta \sim \mathcal{O}(1)$ for Types II and X, and additional large $\tan\beta$ for Type II. Finally the $t\bar{t}$ resonance search excluded small $\tan\beta$ for $m_{H,A} \gtrsim 500$ GeV. There was a loophole. The mass range of $m_{H,A} \approx 350$ – 500 GeV has not been constrained yet by the current LHC heavy Higgs data. In this mass region, both H^0 and A^0 decay dominantly into $t\bar{t}$, but the measurement of the $t\bar{t}$ invariant mass in this range is challenging because the signal events are easily swamped by the background. We need an additional tag for the production of a heavy neutral Higgs boson so that the $t\bar{t}$ resonance search can probe this lower mass region.

Finally we studied whether two diphoton excesses with a 2σ local significance observed by ATLAS can be accommodated in the aligned 2HDM. The $m_{\gamma\gamma} = 200$ GeV resonance can be H^0 , A^0 , or degenerate H^0/A^0 in Types I, II, and Y, with small $\tan\beta$. In Type X, the $\tau^+\tau^-$ results excluded the 200 GeV diphoton resonance for A^0 and degenerate H^0/A^0 . The $m_{\gamma\gamma} = 530$ GeV resonance is impossible in the aligned 2HDM. Not only is the diphoton

rate too small, but the $t\bar{t}$ data exclude the resonance. This cannot be avoided since the $t\bar{t}$ rate is closely related with the $\gamma\gamma$ rate through the loop.

ACKNOWLEDGMENTS

This paper was supported by Konkuk University in 2014.

-
- [1] G. Aad *et al.* (ATLAS Collaboration), *Phys. Lett. B* **716**, 1 (2012); S. Chatrchyan *et al.* (CMS Collaboration), *Phys. Lett. B* **716**, 30 (2012).
- [2] G. Aad *et al.* (ATLAS Collaboration), *Phys. Lett. B* **726**, 88 (2013).
- [3] CMS Collaboration, Report No. CMS-PAS-HIG-13-001.
- [4] K. Cheung, J. S. Lee, and P.-Y. Tseng, *Phys. Rev. D* **90**, 095009 (2014).
- [5] V. Khachatryan *et al.* (CMS Collaboration), *Eur. Phys. J. C* **74**, 3076 (2014).
- [6] K. A. Olive *et al.* (Particle Data Group Collaboration), *Chin. Phys. C* **38**, 090001 (2014).
- [7] M. Baak, J. Cúth, J. Haller, A. Hoecker, R. Kogler, K. Mönig, M. Schott, and J. Stelzer, *Eur. Phys. J. C* **74**, 3046 (2014).
- [8] N. D. Christensen, T. Han, and S. Su, *Phys. Rev. D* **85**, 115018 (2012); P. Bechtle, S. Heinemeyer, O. Stal, T. Stefaniak, G. Weiglein, and L. Zeune, *Eur. Phys. J. C* **73**, 2354 (2013); A. Arbey, M. Battaglia, A. Djouadi, and F. Mahmoudi, *Phys. Lett. B* **720**, 153 (2013); N. D. Christensen, T. Han, Z. Liu, and S. Su, *J. High Energy Phys.* **08** (2013) 019; S. F. King, M. Muhlleitner, R. Nevzorov, and K. Walz, *Nucl. Phys.* **B870**, 323 (2013); T. Hahn, S. Heinemeyer, W. Hollik, H. Rzehak, and G. Weiglein, *Phys. Rev. Lett.* **112**, 141801 (2014); P. Ko, Y. Omura, and C. Yu, *Phys. Lett. B* **717**, 202 (2012); *J. High Energy Phys.* **01** (2014), 016; **11** (2014), 054; [arXiv:1502.00262](#).
- [9] G. Belanger, B. Dumont, U. Ellwanger, J. F. Gunion, and S. Kraml, *Phys. Rev. D* **88**, 075008 (2013); K. Cheung, J. S. Lee, and P. Y. Tseng, *J. High Energy Phys.* **05** (2013) 134; C. W. Chiang and K. Yagyu, *J. High Energy Phys.* **07** (2013) 160; B. Grinstein and P. Uttayarat, *J. High Energy Phys.* **06** (2013) 094; **09** (2013) 110(E); O. Eberhardt, U. Nierste, and M. Wiebusch, *J. High Energy Phys.* **07** (2013) 118; A. Celis, V. Ilisie, and A. Pich, *J. High Energy Phys.* **07** (2013) 053; A. Broggio, E. J. Chun, M. Passera, K. M. Patel, and S. K. Vempati, *J. High Energy Phys.* **11** (2014) 058.
- [10] H. S. Cheon and S. K. Kang, *J. High Energy Phys.* **09** (2013) 085; S. Chang, S. K. Kang, J. P. Lee, K. Y. Lee, S. C. Park, and J. Song, *J. High Energy Phys.* **05** (2013) 075.
- [11] S. Chang, S. K. Kang, J. P. Lee, K. Y. Lee, S. C. Park, and J. Song, *J. High Energy Phys.* **09** (2014) 101.
- [12] ATLAS Collaboration, Report Nos. ATLAS-CONF-2013-013; ATLAS-COM-CONF-2013-018; CMS Collaboration, Report No. CMS-PAS-HIG-13-002.
- [13] CMS Collaboration, Report No. CMS-PAS-HIG-13-014.
- [14] ATLAS Collaboration, Report Nos. ATLAS-CONF-2013-067; ATLAS-COM-CONF-2013-082; CMS Collaboration, Report No. CMS-PAS-HIG-13-008.
- [15] G. Aad *et al.* (ATLAS Collaboration), *Phys. Rev. D* **91**, 052007 (2015); C. Vuosalo (CMS Collaboration), *EPJ Web Conf.* **60**, 17001 (2013).
- [16] ATLAS Collaboration, Report Nos. ATLAS-CONF-2014-049; ATLAS-COM-CONF-2014-062.
- [17] P. Turner (CMS Collaboration), [arXiv:1310.7859](#); B. A. Gonzalez, [arXiv:1409.3340](#).
- [18] G. Aad *et al.* (ATLAS Collaboration), *Phys. Rev. Lett.* **113**, 171801 (2014).
- [19] CMS Collaboration, Report No. CMS-PAS-HIG-14-006.
- [20] J. F. Gunion and H. E. Haber, *Phys. Rev. D* **67**, 075019 (2003); G. C. Branco, P. M. Ferreira, L. Lavoura, M. N. Rebelo, M. Sher, and J. P. Silva, *Phys. Rep.* **516**, 1 (2012).
- [21] N. Craig, J. Galloway, and S. Thomas, [arXiv:1305.2424](#); A. Celis, V. Ilisie, and A. Pich, *J. High Energy Phys.* **12** (2013) 095; L. Wang and X. F. Han, *J. High Energy Phys.* **04** (2014) 128; P. S. B. Dev and A. Pilaftsis, *J. High Energy Phys.* **12** (2014) 024.
- [22] B. Dumont, J. F. Gunion, Y. Jiang, and S. Kraml, *Phys. Rev. D* **90**, 035021 (2014).
- [23] C. Y. Chen, S. Dawson, and M. Sher, *Phys. Rev. D* **88**, 015018 (2013); J. Baglio, O. Eberhardt, U. Nierste, and M. Wiebusch, *Phys. Rev. D* **90**, 015008 (2014); C. Lange (ATLAS Collaboration and CMS Collaboration), [arXiv:1411.7279](#); L. Wang and X. F. Han, *J. High Energy Phys.* **05** (2015) 039; B. Holdom and M. Ratzlaff, *Phys. Rev. D* **91**, 035031 (2015).
- [24] S. L. Glashow and S. Weinberg, *Phys. Rev. D* **15**, 1958 (1977); E. A. Paschos, *Phys. Rev. D* **15**, 1966 (1977).
- [25] M. Aoki, S. Kanemura, K. Tsumura, and K. Yagyu, *Phys. Rev. D* **80**, 015017 (2009).
- [26] L. Wang and X. F. Han, *J. High Energy Phys.* **11** (2014) 085; S. Kanemura, H. Yokoya, and Y. J. Zheng, *Nucl. Phys.* **B886**, 524 (2014); B. Coleppa, F. Kling, and S. Su, *J. High Energy Phys.* **01** (2014) 161.
- [27] J. Gunion *et al.*, *The Higgs Hunter's Guide* (Addison-Wesley, New York, 1990).

- [28] P. H. Chankowski, M. Krawczyk, and J. Zochowski, *Eur. Phys. J. C* **11**, 661 (1999).
- [29] A. Djouadi, *Phys. Rep.* **459**, 1 (2008).
- [30] J. Bijnens, J. Lu, and J. Rathsmann, *J. High Energy Phys.* **05** (2012) 118; W. S. Hou and R. S. Willey, *Phys. Lett. B* **202**, 591 (1988); B. Grinstein and M. B. Wise, *Phys. Lett. B* **201**, 274 (1988); B. Grinstein, R. P. Springer, and M. B. Wise, *Nucl. Phys.* **B339**, 269 (1990); V. D. Barger, J. L. Hewett, and R. J. N. Phillips, *Phys. Rev. D* **41**, 3421 (1990); S. Bertolini, F. Borzumati, A. Masiero, and G. Ridolfi, *Nucl. Phys.* **B353**, 591 (1991).
- [31] W. S. Hou and R. S. Willey, *Phys. Lett. B* **202**, 591 (1988); B. Grinstein and M. B. Wise, *Phys. Lett. B* **201**, 274 (1988); B. Grinstein, R. P. Springer, and M. B. Wise, *Nucl. Phys.* **B339**, 269 (1990); V. D. Barger, J. L. Hewett, and R. J. N. Phillips, *Phys. Rev. D* **41**, 3421 (1990); S. Bertolini, F. Borzumati, A. Masiero, and G. Ridolfi, *Nucl. Phys.* **B353**, 591 (1991).
- [32] F. Mahmoudi and O. Stal, *Phys. Rev. D* **81**, 035016 (2010).
- [33] M. Jung, A. Pich, and P. Tuzon, *J. High Energy Phys.* **11** (2010) 003.
- [34] S. Schael *et al.* (ALEPH and DELPHI and L3 and OPAL and SLD and LEP Electroweak Working Group and SLD Electroweak Group and SLD Heavy Flavour Group Collaborations), *Phys. Rep.* **427**, 257 (2006).
- [35] J. Bernabeu, A. Pich, and A. Santamaria, *Nucl. Phys.* **B363**, 326 (1991); H. E. Haber and H. E. Logan, *Phys. Rev. D* **62**, 015011 (2000); G. Degrossi and P. Slavich, *Phys. Rev. D* **81**, 075001 (2010).
- [36] A. Arhrib, P. M. Ferreira, and R. Santos, *J. High Energy Phys.* **03** (2014) 053.
- [37] A. D. Martin, W. J. Stirling, R. S. Thorne, and G. Watt, *Eur. Phys. J. C* **63**, 189 (2009).
- [38] M. Spira, [arXiv:hep-ph/9510347](https://arxiv.org/abs/hep-ph/9510347).
- [39] Z. z. Xing, H. Zhang, and S. Zhou, *Phys. Rev. D* **77**, 113016 (2008).
- [40] S. Aoki *et al.*, *Eur. Phys. J. C* **74**, 2890 (2014).
- [41] E. Barberio *et al.* (Heavy Flavor Averaging Group Collaboration), [arXiv:0808.1297](https://arxiv.org/abs/0808.1297).
- [42] S. P. Martin, *Adv. Ser. Dir. High Energy Phys.* **21**, 1 (2010); R. Dermisek, [arXiv:0806.0847](https://arxiv.org/abs/0806.0847).
- [43] B. Grinstein, R. P. Springer, and M. B. Wise, *Nucl. Phys.* **B339**, 269 (1990); A. Ali and C. Greub, *Z. Phys. C* **60**, 433 (1993); M. Misiak, *Nucl. Phys.* **B393**, 23 (1993); **B439**, 461 (E) (1995); A. J. Buras, *Phys. Lett. B* **333**, 476 (1994); G. Cella, G. Curci, G. Ricciardi, and A. Vicere, *Phys. Lett. B* **325**, 227 (1994); M. Ciuchini, E. Franco, G. Martinelli, L. Reina, and L. Silvestrini, *Phys. Lett. B* **334**, 137 (1994); K. Adel and Y. P. Yao, *Phys. Rev. D* **49**, 4945 (1994); C. Greub and T. Hurth, *Phys. Rev. D* **56**, 2934 (1997); C. Bobeth, M. Misiak, and J. Urban, *Nucl. Phys.* **B567**, 153 (2000).
- [44] M. Ciuchini, G. Degrossi, P. Gambino, and G. F. Giudice, *Nucl. Phys.* **B527**, 21 (1998).
- [45] F. Borzumati and C. Greub, *Phys. Rev. D* **58**, 074004 (1998).
- [46] K. G. Chetyrkin, M. Misiak, and M. Munz, *Phys. Lett. B* **400**, 206 (1997); **425**, 414(E) (1998); K. G. Chetyrkin, M. Misiak, and M. Munz, *Nucl. Phys.* **B518**, 473 (1998); P. Gambino, M. Gorbahn, and U. Haisch, *Nucl. Phys.* **B673**, 238 (2003).
- [47] C. Greub, T. Hurth, and D. Wyler, *Phys. Lett. B* **380**, 385 (1996); C. Greub, T. Hurth, and D. Wyler, *Phys. Rev. D* **54**, 3350 (1996); A. J. Buras, A. Czarnecki, M. Misiak, and J. Urban, *Nucl. Phys.* **B611**, 488 (2001); A. J. Buras, A. Czarnecki, M. Misiak, and J. Urban, *Nucl. Phys.* **B631**, 219 (2002).
- [48] M. Misiak *et al.*, *Phys. Rev. Lett.* **98**, 022002 (2007).
- [49] M. Misiak and M. Steinhauser, *Nucl. Phys.* **B764**, 62 (2007).
- [50] T. Hermann, M. Misiak, and M. Steinhauser, *J. High Energy Phys.* **11** (2012) 036.
- [51] B. Aubert *et al.* (BABAR Collaboration), *Phys. Rev. D* **77**, 051103 (2008).
- [52] K. Abe *et al.* (Belle Collaboration), *Phys. Lett. B* **511**, 151 (2001).
- [53] S. Chen *et al.* (CLEO Collaboration), *Phys. Rev. Lett.* **87**, 251807 (2001).
- [54] J. Urban, F. Krauss, U. Jentschura, and G. Soff, *Nucl. Phys.* **B523**, 40 (1998).
- [55] A. Wahab El Kaffas, P. Osland, and O. M. Ogreid, *Phys. Rev. D* **76**, 095001 (2007).
- [56] G. Buchalla, A. J. Buras, and M. E. Lautenbacher, *Rev. Mod. Phys.* **68**, 1125 (1996).
- [57] C. Q. Geng and J. N. Ng, *Phys. Rev. D* **38**, 2857 (1988); **41**, 1715(E) (1990).
- [58] J. Charles, A. Höcker, H. Lacker, S. Laplace, F. R. Diberder, J. Malclés, J. Ocariz, M. Pivk, and L. Roos, *Eur. Phys. J. C* **41**, 1 (2005), updated results and plots available at <http://ckmfitter.in2p3.fr>.
- [59] ATLAS collaboration, Report Nos. ATLAS-CONF-2013-064; ATLAS-COM-CONF-2013-019; CMS Collaboration, Report No. CMS-PAS-PFT-08-001.
- [60] L. Landau, *Doklady Akademii nauk Ukrainskoi SSR Serii A, Fiziko-matematicheskie i tekhnicheskie nauki* **60**, 207 (1948); C. N. Yang, *Phys. Rev.* **77**, 242 (1950); N. M. Kroll and W. Wada, *Phys. Rev.* **98**, 1355 (1955); R. Plano, A. Prodell, N. Samios, M. Schwartz, and J. Steinberger, *Phys. Rev. Lett.* **3**, 525 (1959).